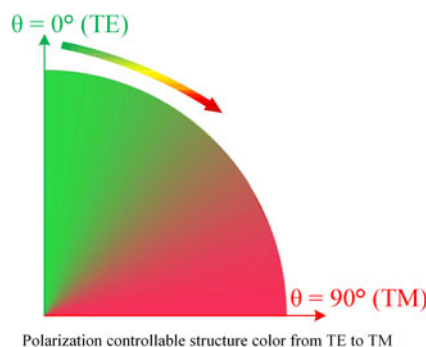


# Wide-Angle Polarization-Controllable Structure Color Based on Metamaterial Resonators With Polarized Multiband Absorption Peaks

Volume 10, Number 3, June 2018

Lei Zhao  
Han Liu  
Zhihong He  
Shikui Dong



---

DOI: 10.1109/JPHOT.2018.2824313  
1943-0655 © 2018 IEEE

# Wide-Angle Polarization-Controllable Structure Color Based on Metamaterial Resonators With Polarized Multiband Absorption Peaks

Lei Zhao, Han Liu, Zhihong He, and Shikui Dong 

School of Energy Science and Engineering, Harbin Institute of Technology, Harbin 150001, China

DOI:10.1109/JPHOT.2018.2824313

1943-0655 © 2018 IEEE. Translations and content mining are permitted for academic research only.  
Personal use is also permitted, but republication/redistribution requires IEEE permission.  
See [http://www.ieee.org/publications\\_standards/publications/rights/index.html](http://www.ieee.org/publications_standards/publications/rights/index.html) for more information.

Manuscript received January 9, 2018; revised March 14, 2018; accepted April 4, 2018. Date of publication April 9, 2018; date of current version May 18, 2018. This work was supported by the National Natural Science Foundation of China (51576054). Corresponding author: Shikui Dong (e-mail: dongsks@hit.edu.cn).

**Abstract:** The polarization-controllable structure color has been theoretically designed by utilizing metamaterial resonators with polarization-dependent multiband absorption peaks. Our designed nanostructure, consisting of the periodic circle and ellipse resonators, shows above 80% reflectivity from 502 to 553 nm (the green structure color) for TE-polarized incident white light, but above 80% reflectivity from 610 to 750 nm (the red structure color) for TM-polarized incident white light. Therefore, the structure colors gradually change from green to red when the polarization angles increasing from 0° (TE) to 90° (TM). The polarization-controllable structure colors come from the polarization-dependent multiband absorption peaks. When the polarization changes from TE to TM, the absorption peaks shift from 454, 624, and 714 nm to 454, 498, and 550 nm. The physical mechanism is explained by the electromagnetic fields distribution and the equivalent *LC* circuit model. It can keep the structure color for a wide incident angle.

**Index Terms:** Subwavelength structure, plasmonics, metamaterial, nanostructures

## 1. Introduction

Color is one of the main information sources for mankind, which depending on the wavelength of light reaching our eyes. The traditional method of changing the color of an object is to cover it with dyes or pigments, which are capable of absorbing some wavelengths of light. The object then displays the unabsorbed color. However, the color can also be manipulated by changing the nanostructure of objects such as birds, marine life, butterflies, and insects in nature [1]–[10]. This phenomenon is often called structure color, which has some distinct advantages such as high stability, easy recycling, high spatial resolution, and small dimension. Inspired by natural structure color, artificial structure color from photonic crystals [11]–[16] have been extensively studied by many scientists. Photonic crystals with the photonic band gap (PGB) can nearly 100% reflect particular wavelengths of light owing to the periodic arrangement of various refractive index dielectric materials [17]–[20]. The interference effect of reflective light determines the visible color.

Unlike the selective reflection in photonic crystals, the selective absorption properties of some nanostructures can also be used to form different structure colors. It has been reported that optical dielectric coating with high absorption on a metallic substrate generates structure color by selectively

absorbing portion of the incident light based on the Fabry-Perot (F-P) effects [21]–[23]. Another promising way to achieve artificial structure color is to take advantage of the Ohmic loss of metals in the plasmonic metamaterial [24]. The metamaterial perfect absorbers (MMPA) [25]–[30] are one kind of plasmonic metamaterials with nearly 100% absorption at the certain wavelength based on the excitation surface plasmon resonances (SPR) and localized surface plasmon resonances (LSPR). It's found that the selective absorption of MMPA can manipulate the reflection spectrum to generate different colors by changing the nanostructure [31]–[33]. Due to the single-band characteristic of most MMPA, the reflective artificial structure colors are usually not the red, green and blue (RGB) but their complementary colors: cyan, magenta, and yellow (CMR).

Compared with the use of dyes and pigments, the structure color possesses the special ability to be manipulated by external stimuli such as solvents [34]–[36], temperature [37]–[39], mechanical force [40]–[42], and incident angle [43]. Polarization is one of the inherent characteristics of light and may provide another degree of freedom to control the structure color through the polarization-controllable MMPA. The 1D polarization-controllable MMPA (such as 1D grating) behaves like a ‘switch’ because it excites only the resonant modes for TE-polarized light [44]–[48]. Cui *et al.* have reported the polarization-controllable structure color based on 1D grating MMPA, which demonstrates some color for TE-polarized incident white light, while white for TM-polarized incident white light [33]. In order to gradually changing the structural color from one color to another (not white), the absorption peak wavelength must be shifted with polarization. For 2D polarization-controllable MMPA, the absorption peak wavelength will shift when the polarization state changes from TE to TM. And this polarization dependent absorption peak wavelength shift (PIAPWS) has been reported in infrared range with the single band [49]–[53]. However, there are few studies on the PIAPWS in the visible region with the multiple bands and their application to the polarization-controllable structure color.

In this paper, we have designed a nanostructure consisting of four layers: a substrate layer on the bottom, a metal layer and a dielectric layer followed, and then a top metal layer with periodic circles and ellipses resonators. The structure is a multiband metamaterial perfect absorber in the visible region with the polarization dependent absorption peak wavelength shift (PIAPWS). So the structure color can be designed into red, green, and blue (RGB) instead of the cyan, magenta, and yellow (CMR). And the structure colors can be actively controlled by the polarization state of the incident light. The physical mechanism of the polarization-controllable multiband absorption is investigated through the electric and magnetic fields distribution and the equivalent LC circuit model. The dependence of the structure color on the incident angles is also studied.

## 2. Structure and Method

The selective reflection of our designed nanostructure comes from the selective absorption of the incident light. Polarization is an inherent characteristic of light and can be used to tune the absorption properties of metamaterial perfect absorbers. So the polarization can actively tune the reflectivity spectrum. The polarization-controllable structure color may be achieved, which is important and have potential applications in many fields like encryption, information storage, decoration, displays, sensors, and camouflage. Our designed periodic nanostructure consists of four layers: a substrate layer on the bottom, a metal layer, and a dielectric layer followed, and then a top metal layer with patterned circles and ellipses, as shown in Fig. 1. The top view of a unit cell is shown in the lower left of Fig. 1. Diameters of the two circles are  $D_1$  and  $D_2$ , respectively. Major axes and minor axes of the two ellipses are  $A_1$ ,  $A_2$ , and  $B_1$ ,  $B_2$ , respectively. The periods in the x and y directions are  $P_x$  and  $P_y$ , respectively. The nanostructure is theoretical analyzed by finite difference time domain (FDTD) method. Silver is chosen as the metal material in the simulation with optical constants taken from the experimental data [54]. Silica is chosen as the dielectric layer with constant permittivity 2.14 in the simulation. Because of the periodicity of the nanostructure, only a unit cell need to be simulated. The periodic boundary condition is used in the x- and y-direction. And the perfect match layer (PML) boundary condition is applied in the z-direction. The absorptivity can be obtained by  $A = 1 - R$  when the bottom silver layer is thick enough to prevent the transmission of incident light.

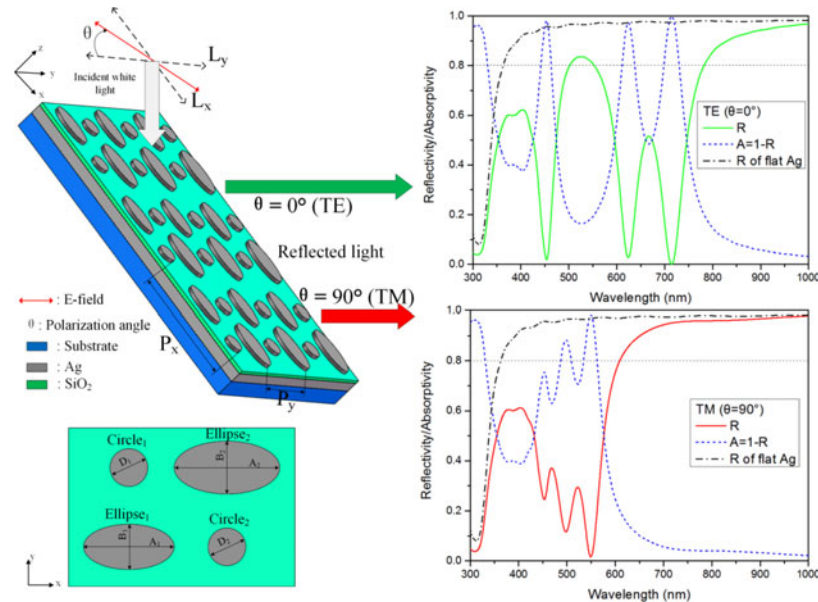


Fig. 1. Three-dimensional sketch of our designed periodic nanostructure and the corresponding reflectivity/absorptivity spectrum for TE and TM incident white light.

Table 1  
The Colors of the Visible Light Spectrum

| Colors | Wavelength | Frequency   |
|--------|------------|-------------|
| Violet | 380-450 nm | 668-789 THz |
| Blue   | 450-475 nm | 631-668 THz |
| Cyan   | 475-495 nm | 606-630 THz |
| Green  | 495-570 nm | 526-606 THz |
| Yellow | 570-590 nm | 508-526 THz |
| Orange | 590-620 nm | 484-508 THz |
| Red    | 620-750 nm | 400-484 THz |

### 3. Results and Discussions

The right side of Fig. 1 shows the reflectivity and absorptivity spectrum for TE-polarized and TM-polarized electromagnetic waves when the x-z plane is the incident plane. The optimized geometry parameters are as follows: P<sub>x</sub> = 0.32 μm, P<sub>y</sub> = 0.224 μm, D<sub>1</sub> = D<sub>2</sub> = 0.06 μm, A<sub>1</sub> = 0.118 μm, B<sub>1</sub> = 0.076 μm, A<sub>2</sub> = 0.12 μm, and B<sub>2</sub> = 0.08 μm. For TE-polarized light, our designed nanostructure shows above 80% reflectivity from 502 to 553 nm, which is right in the green light range (495–570 nm) as shown in Table 1. And the absorptivity spectrum shows three absorption peaks at the wavelength of 454 nm, 624 nm, and 714 nm with absorptivity 98.1%, 97.3%, and 99.9%, respectively. For TM-polarized light, our designed nanostructure shows above 80% reflectivity from 610 to 750 nm, which is right in the red light range (620–750 nm) as shown in Table 1. And the absorptivity spectrum shows three absorption peaks at the wavelength of 454 nm, 498 nm, and 550 nm with absorptivity 75.4%, 88.4%, and 98.4%, respectively. The reflectivity spectrum of Ag film is also calculated and shown in Fig. 1, which displays very high reflectivity for both TE and TM incident light in the whole visible range.

Fig. 2(a) shows the absorptivity spectrum of our designed nanostructure for different polarization angles. It's clear to see that the absorption peak at 454 nm doesn't shift but the absorptivity decrease

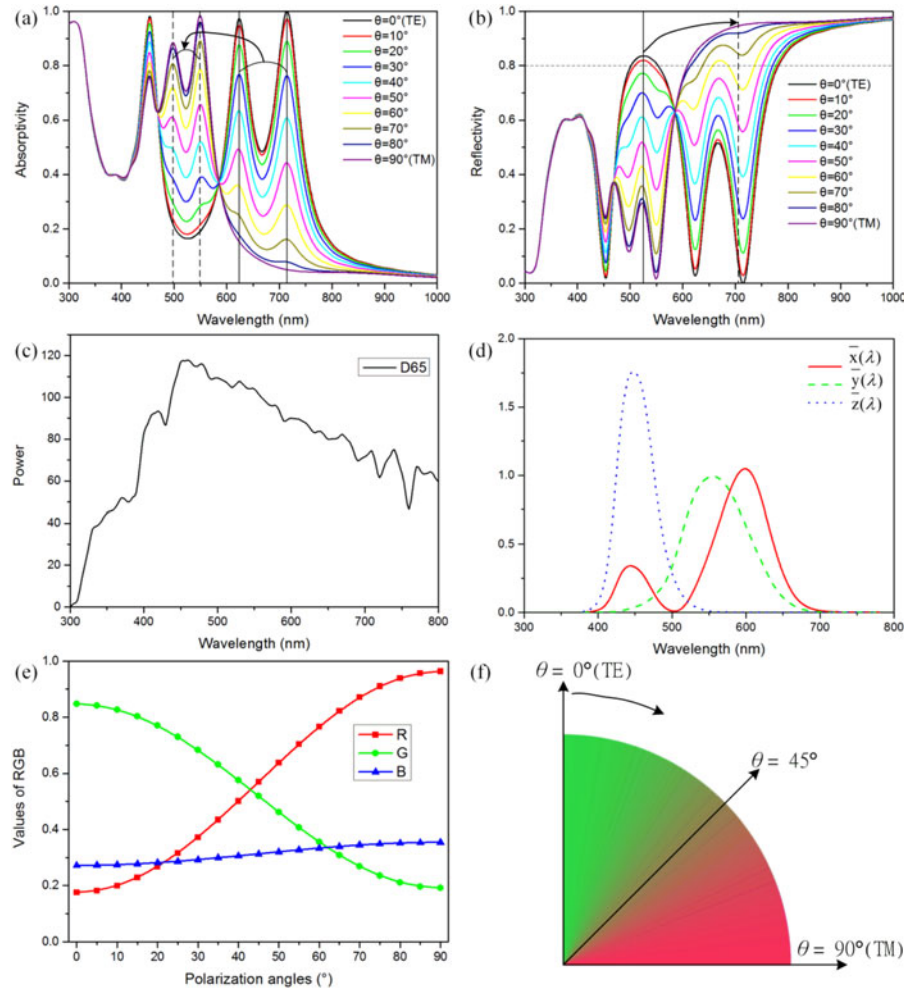


Fig. 2. The (a) absorptivity spectrum and (b) reflectivity spectrum for polarization angles changing from  $0^\circ$  (TE) to  $90^\circ$  (TM) with interval  $10^\circ$ . (c) Spectral power distribution of the CIE normalized illuminant D65. (d) The CIE standard observer color matching functions; (e) The calculated RGB values and (f) corresponding displayed colors for polarization angles changing from  $0^\circ$  (TE) to  $90^\circ$  (TM).

from 98.1% to 75.4%, the absorption peak at 624 nm and 714 nm shift to 498 nm and 550 nm when the polarization angles changing from  $0^\circ$  (TE) to  $90^\circ$  (TM). Due to the polarization dependent absorption peak wavelength shift (PIAPWS), the high reflectivity range also shifts from the green zone to the red zone as shown in Fig. 2(b). To specifically display the color, the RGB values for the spectral reflectivity can be calculated by using the following equations in [55]. We first calculate the XYZ tristimulus values.

$$\begin{aligned}
 X &= \frac{1}{k} \int S(\lambda) R(\lambda) \bar{X}(\lambda) d\lambda \\
 Y &= \frac{1}{k} \int S(\lambda) R(\lambda) \bar{Y}(\lambda) d\lambda \\
 Z &= \frac{1}{k} \int S(\lambda) R(\lambda) \bar{Z}(\lambda) d\lambda \\
 k &= \int S(\lambda) \bar{Y}(\lambda) d\lambda
 \end{aligned} \tag{1}$$

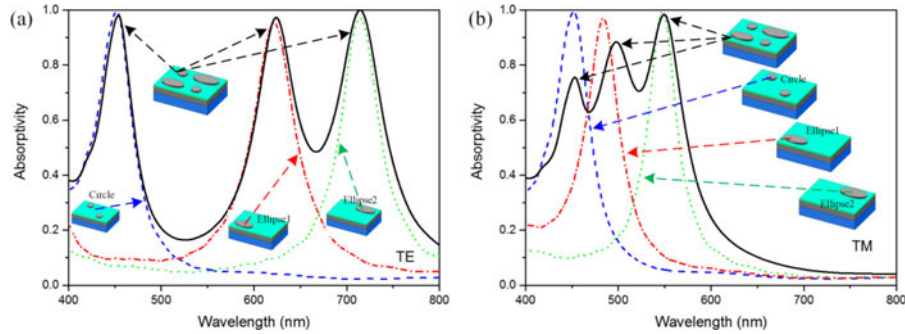


Fig. 3. The spectral absorptivity of four metamaterial perfect absorbers with different nanostructure for (a) TE-polarized and (b) TM-polarized incident light.

Where the  $R(\lambda)$  is the spectral reflectivity; the  $S(\lambda)$  is the spectral power distribution of the CIE normalized illuminant D65 as shown in Fig. 2(c); the  $\bar{x}$ ,  $\bar{y}$ , and  $\bar{z}$  are the CIE standard observer color matching functions as shown in Fig. 2(d). Then, the RGB values can be calculated by:

$$\begin{bmatrix} R \\ G \\ B \end{bmatrix} = \begin{bmatrix} 3.240479 - 1.537105 & -0.498535 \\ -0.9692561.875992 & 0.041556 \\ 0.055648 - 0.204043 & 1.057311 \end{bmatrix} \begin{bmatrix} X \\ Y \\ Z \end{bmatrix} \quad (2)$$

Fig. 2(e) shows the effect of polarization on the RGB values. When the polarization angles increase from 0 to 90, it's clear to see that the B values hardly change because the absorption peak at 454 nm doesn't shift. And the R values increase sharply while the G values drastically decrease because the absorption peak at 624 nm and 714 nm shift to 498 nm and 550 nm. So as shown in Fig. 2(f), the polarization-controllable structure color gradually changes from green to red as the polarization angles from 0° (TE) to 90° (TM). And the polarization-controllable structure color is achieved.

It's already known that the polarization-controllable structure color comes from the polarization-controllable multiband metamaterial perfect absorber (MMPA). And the polarization-controllable MMPA shows some features: the absorption peak at 454 nm doesn't shift while the absorption peaks at 624 nm and 714 nm shift to 478 nm and 550 nm when the polarization angles change from 0° (TE) to 90° (TM). To understand these absorption behaviors, another three MMPAs are theoretical analyzed and the spectral absorptivity is shown in Fig. 3(a) and (b). The MMPA only consisting of two identical circle resonators shows the polarization-insensitive property and the absorption peak keeps at 451 nm for both TE and TM waves. So the absorption peak at 452 nm comes from the circle resonators in our designed nanostructure, which doesn't shift for different polarization angles. The MMPA only consisting of the ellipse<sub>1</sub> resonators shows the polarization-sensitive property. The absorption peak is at 623 nm for TE-polarized wave while at 484 nm for TM-polarized wave. So the absorption peak wavelength shift phenomenon from 624 nm to 498 nm comes from the ellipse<sub>1</sub> resonators in our designed nanostructure. The MMPA only consisting of the ellipse<sub>2</sub> also shows the polarization-sensitive property. The absorption peak is at 714 nm for TE-polarized wave while at 550 nm for TM-polarized wave. So the absorption peak wavelength shift phenomenon from 714 nm to 550 nm comes from the ellipse<sub>2</sub> resonators in our designed nanostructure.

The electric and magnetic field distribution is also investigated to understand the physical mechanism of the polarization-controllable multiband MMPA. Fig. 4(a) shows the electric and magnetic field distribution of absorption peak at 454 nm for TE-polarized incident light. The electric field is mainly localized on the left and right sides of the circle<sub>1</sub> and circle<sub>2</sub>. The y-component of magnetic field is mainly localized between the two circle resonators and the bottom metal, which indicates the excitation of localized surface plasmon polariton (LSPP) mode [25], [26]. Fig. 4(b) shows the

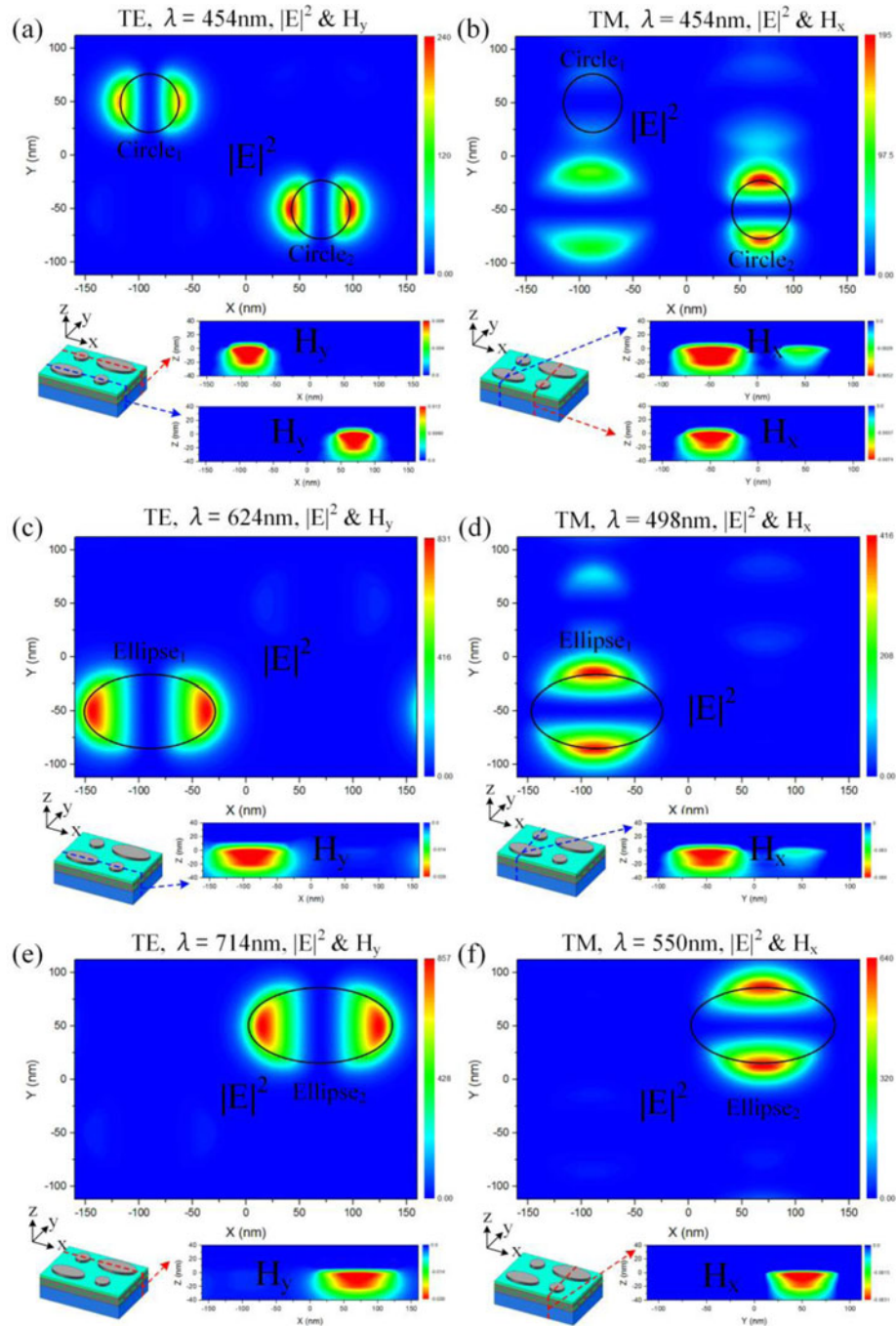


Fig. 4. The electric and magnetic field distribution (a) at 454 nm for TE, (b) at 454 nm for TM, (c) at 624 nm for TE, (d) at 498 nm for TM, (e) at 714 nm for TE, and (f) at 550 nm for TM.

electric and magnetic field distribution of absorption peak at 454 nm for TM-polarized incident light. The electric field intensity is mainly localized on the up and down sides of the circle<sub>2</sub>. The x-component of magnetic field is mainly localized between the circle<sub>2</sub> resonators and the bottom metal, which indicates the excitation of localized surface plasmon polariton (LSPP) mode. So the absorption peak at 452 nm for both TE and TM waves comes from the circle resonators in our designed nanostructure.

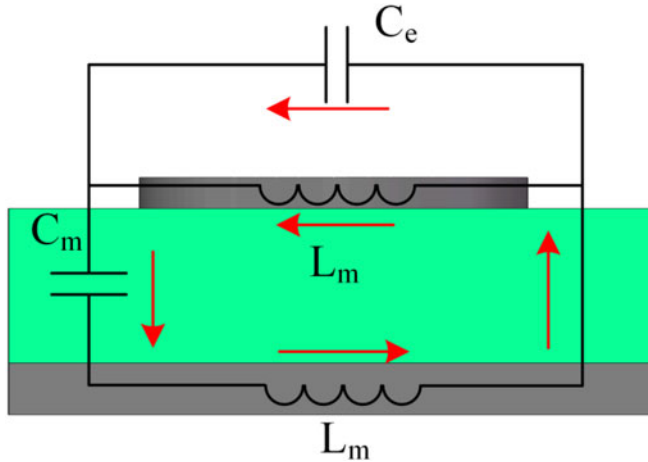


Fig. 5. Schematic of the equivalent LC circuit model. The red arrows represent the direction of electric current.

Fig. 4(c) shows the electric and magnetic field distribution of absorption peak at 624 nm for TE-polarized incident light. The electric field is mainly localized on the left and right sides of the ellipse<sub>1</sub>. The y-component of magnetic field is mainly localized between the ellipse<sub>1</sub> resonators and the bottom metal, which indicates the excitation of localized surface plasmon polariton (LSPP) mode. Fig. 4(d) shows the electric and magnetic field distribution of absorption peak at 498 nm for TM-polarized incident light. The electric field intensity is mainly localized on the up and down sides of the ellipse<sub>1</sub>. The x-component of magnetic field is mainly localized between the ellipse<sub>1</sub> resonators and the bottom metal, which indicates the excitation of localized surface plasmon polariton (LSPP) mode. So the absorption peak wavelength shift phenomenon from 624 nm to 498 nm comes from the ellipse<sub>1</sub> resonators. And the LSPP modes at 624 nm and 498 nm correspond to the major axis A<sub>1</sub> and the minor axis B<sub>1</sub> the ellipse<sub>1</sub>, respectively.

Fig. 4(e) shows the electric and magnetic field distribution of absorption peak at 714 nm for TE-polarized incident light. The electric field is mainly localized on the left and right sides of the ellipse<sub>2</sub>. The y-component of magnetic field is mainly localized between the ellipse<sub>2</sub> resonators and the bottom metal, which indicates the excitation of localized surface plasmon polariton (LSPP) mode. Fig. 4(f) shows the electric and magnetic field distribution of absorption peak at 550 nm for TM-polarized incident light. The electric field intensity is mainly localized on the up and down sides of the ellipse<sub>2</sub>. The x-component of magnetic field is mainly localized between the ellipse<sub>2</sub> resonators and the bottom metal, which indicates the excitation of localized surface plasmon polariton (LSPP) mode. So the absorption peak wavelength shift phenomenon from 714 nm to 550 nm comes from the ellipse<sub>2</sub> resonators. And the LSPP modes at 714 nm and 550 nm correspond to the major axis A<sub>2</sub> and the minor axis B<sub>2</sub> the ellipse<sub>2</sub>, respectively.

Additionally, the LC equivalent circuit model [51]–[53] can be used to explain the performance of the polarization-controllable multiband MMA. Now we consider a simple nanostructure only including the circle resonators with radius r, thickness t. And the period is p, the thickness of the dielectric layer is d. The equivalent LC circuit model is shown in Fig. 5. The gap capacitance C<sub>e</sub> between the neighboring circle resonators is estimated by  $C_e = \varepsilon_0 \pi r t / (p - 2r)$  where the  $\varepsilon_0$  is the free-space permittivity. The capacitance C<sub>m</sub> between the circle resonators and the bottom metal is estimated by  $C_m = c_1 \varepsilon_d \varepsilon_0 \pi r^2 / d$ , where the  $\varepsilon_d$  is the relative permittivity of the middle dielectric layer and c<sub>1</sub> is a numerical factor. The mutual inductance L<sub>m</sub> of the top and bottom metal is estimated by  $L_m = 0.5 \mu_0 \pi d$ , where the  $\mu_0$  is the vacuum permeability. The total impedance of the LC circuit model is given by

$$Z = \frac{i\omega L_m}{1 - \omega^2 L_m C_e} - \frac{2i}{\omega C_m} + i\omega L_m \quad (3)$$

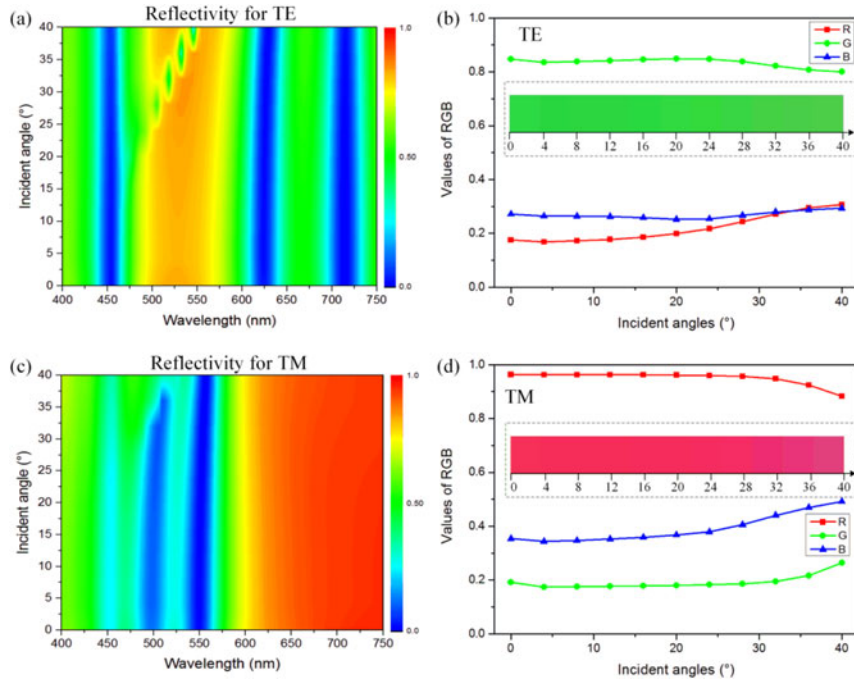


Fig. 6. (a) The spectral reflectivity, (b) calculated RGB values and displayed colors for TE as functions of the incident angles. (c) The spectral reflectivity, (d) calculated RGB values and displayed colors for TM as functions of the incident angles.

Therefore, the magnetic resonance condition can be satisfied when  $Z = 0$ . The resonant frequency can be expressed as

$$\omega_r = \sqrt{\frac{C_m + C_e - (C_m^2 + C_e^2)^{1/2}}{L_m C_m C_e}} \quad (4)$$

Since the influence of  $C_e$  ( $C_e \approx 0.1 C_m$ ) in the LC circuit model is small, the resonant frequency is approximated as  $\omega_r \approx 1/\sqrt{L_m C_m}$ . And the resonant wavelength can be expressed as

$$\lambda_r = \frac{2\pi c}{\omega_r} \approx 2\pi c \sqrt{L_m C_m} \approx 2\pi^2 \sqrt{0.5 c_1 \varepsilon_d} r \propto r \quad (5)$$

where  $c$  is the speed of light. So the resonant wavelength for the circle resonators is approximately proportional to the diameter. As shown in Fig. 4, the electric field distribution of ellipse resonators is mainly localized along the major axis for the TE-polarized incident light, which indicates that the ellipse resonator for TE can be approximately seen as a circle resonator with effective diameter A. Similarly, the ellipse resonator for TM can be approximately seen as a circle resonator with effective diameter B. Then the MMA consisting of the ellipse resonators can be controlled by the polarization. So the absorption peaks at 454 nm, 498 nm, 550 nm, 624 nm, 714 nm can be approximately seen as the results of circle resonators with effective diameters  $D_1$  (0.06  $\mu\text{m}$ ),  $B_1$  (0.076),  $B_2$  (0.08  $\mu\text{m}$ ),  $A_1$  (0.118  $\mu\text{m}$ ),  $A_2$  (0.12  $\mu\text{m}$ ), respectively.

The dependence of polarization-controllable structure color on the incident angle is further studied. With increasing the incident angle from  $0^\circ$  to  $40^\circ$  for TE-polarized light, the high reflectivity range maintains in the green light zone but with a little bit fluctuation as shown in Fig. 6(a). The calculated RGB values shown in Fig. 6(b) hardly changes. So the displayed color keeps green for TE light. Fig. 6(c) and (d) present the reflectivity spectrum and corresponding RGB values and displayed colors for TM-polarized light as functions of incident angles. It's clear to see that the high

reflectivity range keeps in the red light zone but the reflectivity of the left spectral range has a little increase. Although the RGB values have a little fluctuation, the displayed color can still maintain the red for wide angles. So our designed polarization-controllable structure colors can maintain for wide incident angles.

#### 4. Conclusion

In summary, we have designed the polarization-controllable structure color by utilizing metamaterial resonators with polarization dependent multiband absorption peaks. Our designed nanostructure consists of periodic circle and ellipse resonators. The structure can show the three primary colors of red, green, and blue (RGB). And the structure colors can be actively controlled by the polarization state of the incident light. The nanostructure shows above 80% reflectivity from 502 to 553 nm (green) for TE but from 610 to 750 nm (red) for TM, which comes from the polarization dependent multiband absorption peaks shifting from 454 nm, 624 nm, and 714 nm to 454 nm, 498 nm, and 550 nm. So the structure colors gradually change from green to red when the polarization angles increasing from 0° (TE) to 90° (TM). The high absorptivity in our nanostructure comes from the excitation of localized surface plasmon polariton (LSPP) mode. Furthermore, the structure colors hardly change for both TE and TM when the incident angle is less than 30 degrees.

---

#### References

- [1] M. F. Land, "A multilayer interference reflector in the eye of the scallop, *pecten maximus*," *J. Exp. Biol.*, vol. 45, pp. 433–447, 1966.
- [2] Y. Zhao, Z. Xie, H. Gu, C. Zhu, and Z. Gu, "Bio-inspired variable structural color materials," *Chem. Soc. Rev.*, vol. 41, no. 8, pp. 3297–3317, 2012.
- [3] S. Kinoshita and S. Yoshioka, "Structural colors in nature: The role of regularity and irregularity in the structure," *Chem. Phys. Chem.*, vol. 6, no. 8, pp. 1443–1459, 2005.
- [4] P. Vukusic and J. R. Sambles, "Photonic structures in biology," *Nature*, vol. 424, pp. 852–855, Aug. 2003.
- [5] F. Liu, B. Q. Dong, X. H. Liu, Y. M. Zheng, and J. Zi, "Structural color change in longhorn beetles *Tmesisternus isabellae*," *Opt. Exp.*, vol. 17, no. 18, pp. 16183–16191, Aug. 2009.
- [6] F. Liu, B. Dong, F. Zhao, X. Hu, X. Liu, and J. Zi, "Ultraneegative angular dispersion of diffraction in quasiordered biophotonic structures," *Opt. Exp.*, vol. 19, no. 8, pp. 7750–7755, Apr. 2011.
- [7] J. W. Galusha, L. R. Richey, J. S. Gardner, J. N. Cha, and M. H. Bartl, "Discovery of a diamond-based photonic crystal structure in beetle scales," *Phys. Rev. E*, vol. 77, no. 5, May 2008, Art. no. 050904.
- [8] S. Vignolini *et al.*, "Pointillist structural color in *pollia fruit*," *Proc. Nat. Acad. Sci.*, vol. 109, no. 39, pp. 15712–15715, Aug. 2012.
- [9] H. Yin *et al.*, "Iridescence in the neck feathers of domestic pigeons," *Phys. Rev. E*, vol. 74, no. 5, Nov. 2006, Art. no. 051916.
- [10] F. Liu *et al.*, "Inconspicuous structural coloration in the elytra of beetles *Chlorophila obscuripennis* (Coleoptera)," *Phys. Rev. E*, vol. 77, no. 1, Jan. 2008, Art. no. 012901.
- [11] Z. Wang *et al.*, "Bioinspired water-vapor-responsive organic/inorganic hybrid one-dimensional photonic crystals with tunable full-color stop band," *Adv. Funct. Mater.*, vol. 20, no. 21, pp. 3784–3790, 2010.
- [12] E. Kim, S. Y. Kim, G. Jo, S. Kim, and M. J. Park, "Colorimetric and resistive polymer electrolyte thin films for real-time humidity sensors," *ACS Appl. Mater. Interfaces*, vol. 4, no. 10, pp. 5179–5187, Sep. 2012.
- [13] E. Tian, J. Wang, Y. Zheng, Y. Song, L. Jiang, and D. Zhu, "Colorful humidity sensitive photonic crystal hydrogel," *J. Mater. Chem.*, vol. 18, no. 10, pp. 1116–1122, Jan. 2008.
- [14] M. M. Hawkeye and M. J. Brett, "Optimized colorimetric photonic-crystal humidity sensor fabricated using glancing angle deposition," *Adv. Funct. Mater.*, vol. 21, no. 19, pp. 3652–3658, 2011.
- [15] Y. Kang, J. J. Walish, T. Gorishny, and E. L. Thomas, "Broad-wavelength-range chemically tunable block-copolymer photonic gels," *Nature Mater.*, vol. 6, no. 12, pp. 957–960, Oct. 2007.
- [16] C. Fenzl, S. Wilhelm, T. Hirsch, and O. S. Wolfbeis, "Optical sensing of the ionic strength using photonic crystals in a hydrogel matrix," *ACS Appl. Mater. Interfaces*, vol. 5, no. 1, pp. 173–178, Dec. 2013.
- [17] H. Saito, Y. Takeoka, and M. Watanabe, "Simple and precision design of porous gel as a visible indicator for ionic species and concentration," *Chem. Commun.*, vol. 81, no. 17, pp. 2126–2127, Jul. 2003.
- [18] Y. J. Lee and P. V. Braun, "Tunable inverse opal hydrogel pH sensors," *Adv. Mater.*, vol. 15, no. 78, pp. 563–566, Apr. 2003.
- [19] Q. Cui, W. Wang, B. Gu, and L. Liang, "A combined physical-chemical polymerization process for fabrication of nanoparticle-hydrogel sensing materials," *Macromolecules*, vol. 45, no. 20, pp. 8382–8386, Oct. 2012.
- [20] H. S. Lim, J. H. Lee, J. J. Walish, and E. L. Thomas, "Dynamic swelling of tunable full-color block copolymer photonic gels via counterion exchange," *ACS Nano*, vol. 6, no. 10, pp. 8933–8939, Sep. 2012.
- [21] M. A. Kats, R. Blanchard, P. Genevet, and F. Capasso, "Nanometre optical coatings based on strong interference effects in highly absorbing media," *Nature Mater.*, vol. 12, no. 1, pp. 20–24, Jan. 2013.

- [22] W. Streyer, S. Law, G. Rooney, T. Jacobs, and D. Wasserman, "Strong absorption and selective emission from engineered metals with dielectric coatings," *Opt. Exp.*, vol. 21, no. 7, pp. 9113–9122, Apr. 2013.
- [23] M. A. Kats, R. Blanchard, S. Ramanathan, and F. Capasso, "Thin-film interference in lossy, ultra-thin layers," *Opt. Photon. News*, vol. 25, no. 1, pp. 40–47, Jan. 2014.
- [24] C. M. Soukoulis and M. Wegener, "Past achievements and future challenges in 3D photonic metamaterials," *Nature Photon.*, vol. 5, pp. 523–530, Jul. 2011.
- [25] J. Hao, J. Wang, X. Liu, W. J. Padilla, L. Zhou, and M. Qiu, "High performance optical absorber based on a plasmonic metamaterial," *Appl. Phys. Lett.*, vol. 96, no. 25, Jun. 2010, Art. no. 251104.
- [26] G. Dayal and S. A. Ramakrishna, "Design of highly absorbing metamaterials for infrared frequencies," *Opt. Exp.*, vol. 20, no. 16, pp. 17503–17508, Jul. 2012.
- [27] Y. Chen, J. Dai, M. Yan, and M. Qiu, "Honeycomb-lattice plasmonic absorbers at NIR: Anomalous high-order resonance," *Opt. Exp.*, vol. 21, no. 18, p. 20873–20879, Aug. 2013.
- [28] S. Luo, J. Zhao, D. Zuo, and X. Wang, "Perfect narrow band absorber for sensing applications," *Opt. Exp.*, vol. 24, no. 9, p. 9288–9294, Apr. 2016.
- [29] K. Q. Le, Q. M. Ngo, and T. K. Nguyen, "Nanostructured metal–insulator– metal metamaterials for refractive index biosensing applications: Design, fabrication, and characterization," *IEEE J. Sel. Topics Quantum Electron.*, vol. 23, no. 2, Apr. 2017, Art. no. 6900506.
- [30] C. Chen and W. Jun, "Computational and experimental verification of a wide-angle metamaterial absorber," *Chin. Phys. B*, vol. 26, no. 4, Feb. 2017, Art. no. 044101.
- [31] K. Kumar, H. Duan, R. S. Hegde, S. C. W. Koh, J. N. Wei, and J. K. W. Yang, "Printing colour at the optical diffraction limit," *Nature Nanotechnol.*, vol. 7, no. 9, pp. 557–561, Aug. 2012.
- [32] A. S. Roberts, A. Pors, O. Albrektsen, and S. I. Bozhevolnyi, "Subwavelength plasmonic color printing protected for ambient use," *Nano Lett.*, vol. 14, no. 2, pp. 783–787, Jan. 2014.
- [33] J. Cui, X.-C. Cui, H. Xu, Y. Liu, J. Zheng, and Z.-C. Ye, "Polarized structure color from thin dielectric gratings on a metal film," *Appl. Opt.*, vol. 54, no. 13, pp. 3868–3872, May 2015.
- [34] H. Li, L. Chang, J. Wang, L. Yang, and Y. Song, "A colorful oil-sensitive carbon inverse opal," *J. Mater. Chem.*, vol. 18, no. 42, pp. 5098–5103, Sep. 2008.
- [35] I. B. Burgess, L. Mishchenko, B. D. Hatton, M. Kolle, M. Lončar, and J. Aizenberg, "Encoding complex wettability patterns in chemically functionalized 3D photonic crystals," *J. Amer. Chem. Soc.*, vol. 133, no. 32, pp. 12430–12432, Jul. 2011.
- [36] S. Colodrero, M. Ocana, and H. Miguez, "Nanoparticle-based one-dimensional photonic crystals," *Langmuir*, vol. 24, no. 9, pp. 4430–4434, Feb. 2008.
- [37] M. C. Chiappelli and R. C. Hayward, "Photonic multilayer sensors from photo-crosslinkable polymer films," *Adv. Mater.*, vol. 24, no. 45, pp. 6100–6104, 2012.
- [38] I. Pavlichenko, A. T. Exner, M. Guehl, P. Lugli, G. Scarpa, and B. V. Lotsch, "Humidity-enhanced thermally tunable TiO<sub>2</sub>/SiO<sub>2</sub> Bragg stacks," *J. Phys. Chem. C*, vol. 116, no. 1, pp. 298–305, 2012.
- [39] Y. Hu, J. Wang, H. Wang, Q. Wang, J. Zhu, and Y. Yang, "Microfluidic fabrication and thermoreversible response of core/shell photonic crystalline microspheres based on deformable nanogels," *Langmuir*, vol. 28, no. 49, pp. 17186–17192, Nov. 2012.
- [40] G. A. Ozin and A. C. Arsenault, "P-Ink and Elast-Ink from lab to market," *Mater. Today*, vol. 11, nos. 7/8, pp. 44–51, 2008.
- [41] E. P. Chan, J. J. Walish, E. L. Thomas, and C. M. Stafford, "Block copolymer photonic gel for mechanochromic sensing," *Adv. Mater.*, vol. 23, no. 40, pp. 4702–4706, 2011.
- [42] B. Viel, T. Ruhl, and G. P. Hellmann, "Reversible deformation of opal elastomers," *Chem. Mater.*, vol. 19, no. 23, pp. 5673–5679, Oct. 2007.
- [43] G. Si, Y. Zhao, E. S. P. Leong, J. Lv, and Y. J. Liu, "Incident-angle dependent color tuning from a single plasmonic chip," *Nanotechnology*, vol. 25, no. 45, Oct. 2014, Art. no. 455203.
- [44] C. Wu *et al.*, "Large-area wide-angle spectrally selective plasmonic absorber," *Phys. Rev. B*, vol. 84, no. 7, Aug. 2011, Art. no. 075102.
- [45] L. Meng, D. Zhao, Q. Li, and M. Qiu, "Polarization-sensitive perfect absorbers at near-infrared wavelengths," *Opt. Exp.*, vol. 21, no. S1, pp. A111–A122, Dec. 2012.
- [46] X. Xiong *et al.*, "Polarization-dependent perfect absorbers/reflectors based on a three-dimensional metamaterial," *Phys. Rev. B, Condens. Matter Mater. Phys.*, vol. 88, no. 11, Sep. 2013, Art. no. 115105.
- [47] S. Ogawa, Y. Takagawa, and M. Kimata, "Polarization-selective uncooled infrared sensor using a one-dimensional plasmonic grating absorber," *Proc. SPIE*, vol. 9451, 2015, Art. no. 94511K.
- [48] J. Tang, Z. Xiao, K. Xu, X. Ma, and Z. Wang, "Polarization-controlled metamaterial absorber with extremely bandwidth and wide incidence angle," *Plasmonics*, vol. 11, no. 5, pp. 1393–1399, Mar. 2016.
- [49] K. Chen, R. Adato, and H. Altug, "Dual-band perfect absorber for multispectral plasmon-enhanced infrared spectroscopy," *ACS Nano*, vol. 6, no. 9, pp. 7998–8006, Aug. 2012.
- [50] Y. Li, B. Wang, and X. Xu, "Polarization sensitivity contributes to multiple band spectra of one mid-infrared absorber," *Chin. Opt. Lett.*, vol. 12, no. 10, Oct. 2014, Art. no. 101603.
- [51] A. Sakurai, B. Zhao, and Z. M. Zhang, "Effect of polarization on dual-band infrared metamaterial emitters or absorbers," *J. Quant. Spectrosc. Radiat. Transf.*, vol. 158, pp. 111–118, 2015.
- [52] B. X. Khuyen *et al.*, "Size-efficient metamaterial absorber at low frequencies: Design, fabrication, and characterization," *J. Appl. Phys.*, vol. 117, no. 24, Jun. 2015, Art. no. 243105.
- [53] N. Chen *et al.*, "Polarization controllable multispectral symmetry-breaking absorber in mid-infrared," *J. Appl. Phys.*, vol. 120, Aug. 2016, Art. no. 063105.
- [54] Palik, E. D., *Handbook of Optical Constants of Solids*, vol. 3. New York, NY, USA: Academic, 1998, pp. 286–295.
- [55] Commission Internationale de l'Eclairage, "Colorimetry," 3rd ed. CIE, Vienna, Austria, Tech. Rep. CIE 15:2004, 2004.